Elastic and thermal properties of free-standing molybdenum disulfide membranes measured using ultrafast transient grating spectroscopy

Taeyong Kim, , Ding Ding, , Jong-Hyuk Yim, , Young-Dahl Jho, and , and Austin J. Minnich

Citation: APL Materials **5**, 086105 (2017); doi: 10.1063/1.4999225
View online: http://dx.doi.org/10.1063/1.4999225
View Table of Contents: http://aip.scitation.org/toc/apm/5/8
Published by the American Institute of Physics

APL MATERIALS **5**, 086105 (2017)

Elastic and thermal properties of free-standing molybdenum disulfide membranes measured using ultrafast transient grating spectroscopy

Taeyong Kim,[1,a] Ding Ding,[2,a] Jong-Hyuk Yim,[3] Young-Dahl Jho,[3,b] and Austin J. Minnich[1,c]

[1]*Division of Engineering and Applied Science, California Institute of Technology, Pasadena, California 91125, USA*

[2]*Singapore Institute of Manufacturing Technology, 2 Fusionopolis Way, Singapore 138634, Singapore*

[3]*School of Electrical Engineering and Computer Science, Gwangju Institute of Science and Technology, Gwangju 61005, South Korea*

(Received 25 April 2017; accepted 2 August 2017; published online 21 August 2017)

Molybdenum disulfide (MoS_2), a member of transition-metal dichalcogenide family, is of intense interest due to its unique electronic and thermoelectric properties. However, reports of its in-plane thermal conductivity vary due to the difficulty of in-plane thermal conductivity measurements on thin films, and an experimental measurement of the in-plane sound velocity has not been reported. Here, we use time-resolved transient grating spectroscopy to simultaneously measure the in-plane elastic and thermal properties of free-standing MoS_2 membranes at room temperature. We obtain a longitudinal acoustic phonon velocity of 7000 ± 40 m s^{-1} and an in-plane thermal conductivity of 74 ± 21 W $m^{-1}K^{-1}$. Our measurements provide useful insights into the elastic and thermal properties of MoS_2 and demonstrate the capability of transient grating spectroscopy to investigate the in-plane vibrational properties of van der Waals materials that are challenging to characterize with conventional methods. © *2017 Author(s). All article content, except where otherwise noted, is licensed under a Creative Commons Attribution (CC BY) license (http://creativecommons.org/licenses/by/4.0/).*
[http://dx.doi.org/10.1063/1.4999225]

Transition-metal dichalcogenides (TMDCs) are of considerable interest due to their unique layer-thickness-dependent electronic properties and robust thermal stability.[1–5] In particular, molybdenum disulfide (MoS_2), a member of the TMDC family, has been extensively investigated due to its potential applications in electronics, photovoltaics, and thermoelectrics.[6–9] In addition to its intriguing electronic properties such as high electron mobility (up to 200 cm^2 V^{-1} s^{-1}) and indirect-to-direct transition of bandgap with reduced dimensionality,[6,9] MoS_2 has further revealed promising thermoelectric features such as high Seebeck coefficient.[10]

Thermal transport in MoS_2 is therefore of intense interest. However, theoretical and experimental studies report a broad range of in-plane thermal conductivity values of MoS_2. For example, calculations of the in-plane thermal conductivity κ of monolayer MoS_2 vary from 19.76 to 155 W $m^{-1}K^{-1}$.[10–18] Various experimental techniques, including Raman spectroscopy, thermal bridge, and time-resolved magneto-optical Kerr effect (TR-MOKE), have been applied to measure the κ of monolayer, few layer, and bulk MoS_2. The reported values vary widely; from 30.5 to 101 W $m^{-1}K^{-1}$ for monolayers,[19–21] 52–102 W $m^{-1}K^{-1}$ for few layers,[19,22,23] and 85–110 W $m^{-1}K^{-1}$ for bulk.[24]

At the same time, the elastic and acoustic properties of MoS_2 have also been studied, motivated by applications such as flexible electronics.[25–29] In particular, the cross-plane longitudinal sound velocity of MoS_2 has recently been characterized by a transient reflection method.[30] However, although

[a]T. Kim and D. Ding contributed equally to this work.
[b]Author to whom correspondence should be addressed: jho@gist.ac.kr
[c]Author to whom correspondence should be addressed: aminnich@caltech.edu

 © Author(s) 2017

ab initio calculations of in-plane sound velocity have been reported, to the best of our knowledge the value has not been experimentally confirmed.[17,26]

Here, we report measurements of longitudinal acoustic (LA) phonon velocity and in-plane thermal conductivity of free-standing MoS_2 membranes using transient grating (TG) spectroscopy. This non-contact optical method has important advantages over conventional characterization methods in the thermal sciences in that the acoustic and thermal properties can be determined concurrently and that heat primarily flows in one spatial direction, simplifying the data interpretation. We obtain a v_{LA} of 7000 ± 40 m s^{-1} and a corresponding c_{11} elastic constant of 248 GPa, in good agreement with theory; and an in-plane thermal conductivity of 74 ± 21 W $m^{-1}K^{-1}$. These findings provide insight into in-plane thermal and elastic transport in MoS_2 and set the stage for further studies of TMDC films using TG.

We prepared suspended MoS_2 membranes by mechanical exfoliation of bulk crystal MoS_2 (2D Semiconductor Inc.). Silicon-on-insulator (SOI) wafers were wet-etched to create rectangular apertures of dimension about 1–2 mm at the device side of the wafer. Both SOI wafers and bulk MoS_2 were separately cleaned in an ultrasonic bath of acetone for 5 min, then in an ultrasonic bath of methanol for 5 min and finally in an ultrasonic bath of deionized water for 5 min. Then, both wafers and bulk MoS_2 were left in a nitrogen gas flow and annealed at 110 °C during 3 min to dry the samples. Multilayer MoS_2 flakes were then cleaved from the bulk MoS_2 by repeatedly exfoliating with scotch tape. To fix the MoS_2 flake to the SOI wafer, UV curable epoxy was applied on each corner of the rectangular apertures. The flakes were then placed over the aperture in the substrate and were left under UV illumination for 1 min to cure the epoxy.

The membranes were characterized using optical microscopy and transmission electron microscope (TEM). Figure 1(a) shows a confocal microscope image of a sample prepared with this method. The image shows that the membrane is intact with some wrinkles over the clear aperture area. The thickness of the membrane was determined by measuring the transmitted optical power through the membrane. For an incident power of 3 mW at 800 nm, 765 μW was transmitted. Using the Beer-Lambert law and the known dielectric function of MoS_2,[31–33] we estimate the thickness as 5 μm. We also used high resolution TEM to verify the single-crystalline nature of the sample along with selected area electron diffraction of the [001] zone axis to verify the lattice constants, as indicated in Fig. 1(b). We obtained the magnitude of reciprocal lattice vector as 3.7 nm^{-1}, which agrees well with the hexagonal symmetry with lattice spacing of 0.27 nm along the (100) plane as in Fig. 1(b).[34,35]

Next, we performed the TG measurement to obtain in-plane elastic and thermal properties. Detailed discussions of the TG method, including the excitation and detection mechanisms, can be

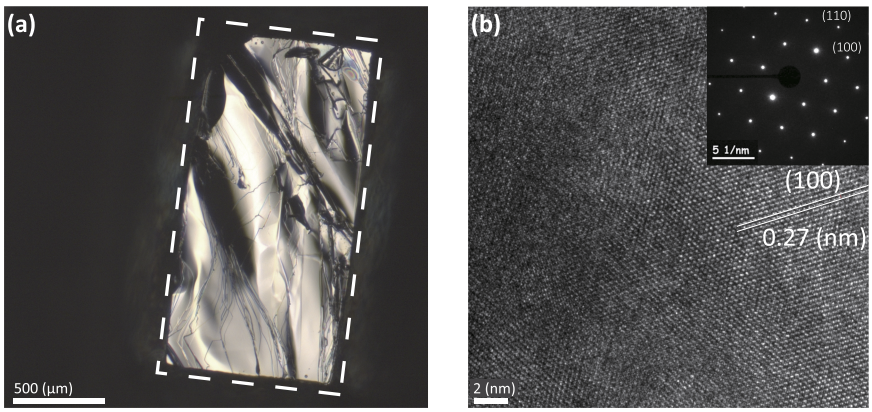

FIG. 1. (a) Confocal optical microscope images of a MoS_2 membrane suspended over a rectangular hole in an SOI wafer. The dimensions of the free-standing area are about 1 × 2 mm^2. The dashed line highlights the area where the membrane is suspended. (b) High resolution transmission electron microscopy (HRTEM) image of MoS_2 indicating single-crystalline structure and revealing the hexagonal lattice. The inset of Fig. 1(b) displays the corresponding selected-area electron diffraction (SAED) pattern along the [001] zone axis. The lattice spacing was identified to be 0.27 nm which is well-matched with the reciprocal lattice distance 3.7 nm^{-1} obtained from SAED.

found elsewhere.[36–38] Our experiment is based on the heterodyne method that measures the coherent interference of the diffracted signal beam and a reference probe beam, leading to substantial increases in signal-to-noise ratio as described in Johnson *et al.*[37]

Briefly, we used a regeneratively amplified Ti:sapphire laser (Libra, Coherent) that generated 100 fs pulses at 10 kHz with an energy of 0.4 mJ. The pulse train, which was centered at 800 nm, was split into pump and probe beams using a half-wave plate and polarizing beam splitter. To spectrally separate pump and probe pulses, a two-tint optical filtering scheme was used: an optical filter was placed along the pump path (single-band band pass filter at 786 nm, Semrock Inc.), and along the probe path and before the detector for suppressing undesirable pump scattering into the detector (RazerEdge long pass filter at 808 nm, Semrock Inc.).[39]

The pump beam was mechanically chopped at 2.5 kHz with a chopper wheel and focused onto a translatable optical phase mask to yield two excitation pulses. The excitation pulses were focused onto a spot with a diameter of 550 μm; their interference generated a periodic heating profile that resulted in thermoelastic standing LA waves and a spatially periodic thermal gradient. The probe beam was directed to a mechanical delay stage (ACT115DL, Aerotech) with a silver coated retro-reflector. The delay stage was arranged to perform a double-pass reflection, providing approximately 4 m of spatial delay corresponding to around 13 ns in time delay. The probe pulses were then directed to the optical phase mask, yielding signal and reference beams. The signal beam passed through a glass window to provide optical phase adjustment and was focused onto the sample; the reference beam was attenuated by a neutral density filter (ND 3) and focused onto the sample. The diameter of the focused probe beam was 400 μm. After transmitting through the sample, the overlap of the transmitted reference and first-order diffracted signal beam were directed to the detector (BPW34, Vishay Inc.). This signal was then balanced by another photodiode measuring a reference beam and the subtracted signal fed into lock-in amplifier (SR 830 of Stanford Research Systems). The relative heterodyned phase difference between the reference beam and the probe beam was controlled by motor controller (DC Stepper Motorized Actuator, Thorlabs).

We conducted measurements with transient grating periods (Λ) varying from 1.89 μm to 7.15 μm at the sample surface. The grating period was calibrated by verifying the acoustic velocity of sound waves in water. Following the procedure described in Johnson *et al.*,[37] experimental data at distinct phase differences between reference and signal beams $\phi_H = 0$ and $\phi_H = \pi$ are subtracted to isolate the thermally induced heterodyned signal. The pump and probe beam powers were set to 15 mW and 6 mW at the sample, respectively. The steady-state and transient temperature rises on the sample are around 6 K and 0.6 K, respectively.

Figure 2 shows two representative heterodyned signals at different transient grating periods. For each measurement, the signals at $\phi_H = 0$ and $\phi_H = \pi$ are clearly superimposable by flipping the sign of one measurement, as expected. The signals at $\phi_H = 0$ and $\phi_H = \pi$ were then subtracted to yield the final signal. As in Figs. 2(c) and 2(f), we observe an initial rise at 0 ns that quickly relaxes away within 2 ns followed by another slower decay with the opposite amplitude sign. We attribute the first relaxation to ambipolar diffusion of photo-generated electrons and holes and the second decay to the thermal and acoustic response of the sample. The thermal decay becomes slower as the grating period increases, as expected.

We fit these experimental data using the formula,

$$f(t) = Ae^{-\frac{t}{\tau_T}} + Be^{-\frac{t}{\tau_S}}\cos(2\pi\nu t + \phi), \tag{1}$$

where the first (second) term represents the thermal (acoustic) signal with amplitude A (B), τ_T and τ_S are the decay time constants for the thermal and acoustic signals, respectively, ν is the frequency of the oscillations, and ϕ is the phase of the oscillation.[40] The frequency of the oscillations ν was first extracted using a Fourier transform [the inset of Figs. 3(a) and 3(b)] and substituted into Eq. (1). The fitting is performed after the electronic relaxation ends, corresponding to a thermalization time of around 2 ns but which increases with the grating period.[40] We obtain the other fitting parameters using least square fitting with the Levenberg-Marquardt algorithm.

The results of the fitting for two grating periods are shown in Figs. 3(a) and 3(b). We observe good agreement between the model and the data. Figure 3(c) visualizes the sensitivity of the solutions of fitted curves to the fitted thermal decay rate. We obtain error bounds on the thermal decay rate

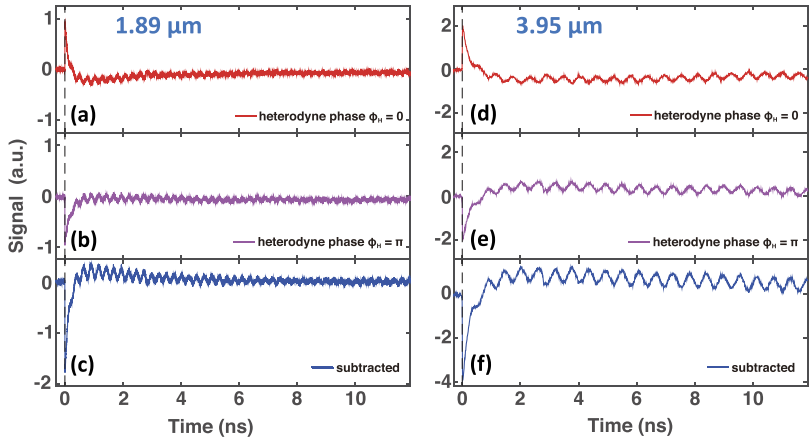

FIG. 2. Signals measured at a grating period of 1.89 μm [(a), (b), and (c)], and 3.95 μm [(d), (e), and (f)]. At each grating period, the signals with optical heterodyne phase of $\phi_H = 0$ [(a) and (d)] and $\phi_H = \pi$ [(b) and (e)] are subtracted to isolate thermally induced signal [(c) and (f)].

by determining by what percentage it can change while still overlapping the data. We find that the noise in the experimental measurements yields fitting uncertainties on the order of 15%.

We first examine the measured acoustic frequency versus grating period, as shown in Fig. 4(a). The acoustic frequency exhibits a linear trend with the inverse grating period, as expected. A linear fit of these data yields an in-plane sound velocity of 7000 ± 40 m s^{-1} and corresponding elastic constant of 248 GPa. The measured elastic constant agrees well with prior theoretical and experimental reports which range from 211 to 240 GPa.[29] Since the membrane is suspended, the corresponding sound velocity is not expected to approach the speed of the Rayleigh mode of the substrate as is the case for a supported membrane. In a free-standing medium, it has been already established that this Lamb wave mode mainly involves intrinsic longitudinal displacements.[36] We note that the Lamb mode originates from thermally induced generation of coherent longitudinal acoustic phonons.[36–38] Our measurement is reasonably close to prior *ab initio* calculations of an in-plane longitudinal acoustic sound velocity of 6500–6700 m s^{-1}.[17,26]

We now examine the thermal properties. Figure 4(b) shows the thermal decay rate versus the square of wavevector. For heat diffusion, this trend should be linear following the relation:

$$\frac{1}{\tau} = \alpha\left(\frac{2\pi}{\Lambda}\right)^2 = \alpha q^2, \tag{2}$$

where τ is the average thermal decay time, α is the in-plane thermal diffusivity, and Λ is the grating period. Equation (2) assumes one-dimensional heat diffusion along the wavevector of TG, a good

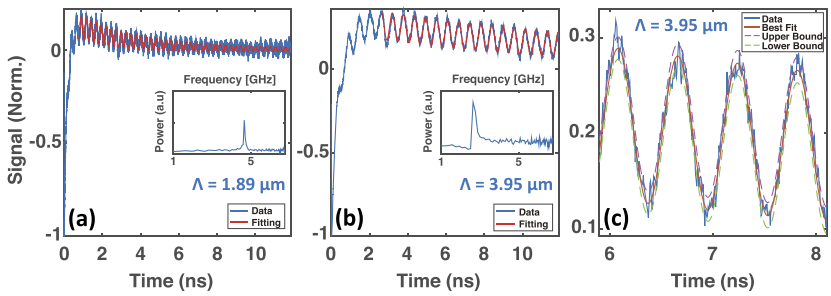

FIG. 3. Signal obtained by the subtraction of heterodyned phase at $\phi_H = 0$ and $\phi_H = \pi$ versus delay time and the model fit at a transient grating period Λ = (a) 1.89 μm and (b) 3.95 μm. Inset: fast Fourier transform of the data showing acoustic oscillation at each grating period. (c) Uncertainty in the fitting curve with respect to the variation of thermal decay rate from (b). The purple (green) line describes lower (upper) bound used to determine the uncertainties. The uncertainty is identified to be on the order of ±15%.

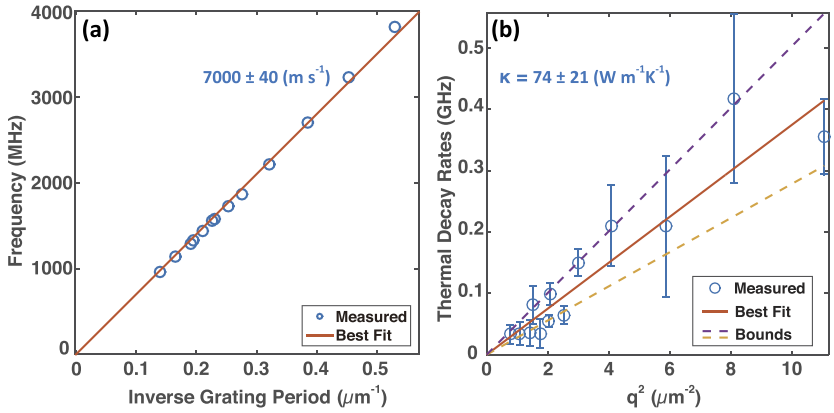

FIG. 4. (a) Measured acoustic frequency versus inverse grating period. The sound velocity is calculated to be 7000 ± 40 m s^{-1}, and the corresponding elastic constant is 248 GPa. (b) Thermal decay rate, or inverse thermal constant, versus wavevector squared. The slope of the dashed line yields the thermal diffusivity value from a linear least square fit. The purple (yellow) dashed line denotes the upper (lower) bound of thermal diffusivity. The thermal conductivity is 74 ± 21 W m^{-1}K^{-1}.

assumption here since the optical penetration depth of MoS_2 at 800 nm (12.5 μm) is longer than the thickness of the sample (5 μm).[31,37]

In Fig. 4(b), we show a linear least square fit from which we obtain the thermal diffusivity. Using a heat capacity from Kim *et al.*,[41] we calculate an in-plane thermal conductivity value of 74 ± 21 W m^{-1}K^{-1}. Our experimental result of thermal conductivity value is slightly lower than recent experimental measurement in Liu *et al.*;[24] which obtained a value of 85 ± 6 W m^{-1}K^{-1} using TR-MOKE. The discrepancy may be due to the differences in sample quality; TG probes a larger thermal length scale than does TR-MOKE and thus is more sensitive to defects. Additionally, defects may have been introduced in our sample preparation procedure. Nevertheless, our value is in reasonable agreement with this prior report.[24] We also tentatively conclude that phonon mean free paths are smaller than the grating periods considered here as the linear trend observed in Fig. 4(b) is characteristic of phonon diffusion.[15,24] However, this conclusion should be re-examined with measurements of smaller uncertainty than those presented here. Moreover, our experimental observations are well supported by some of previous theoretical predictions on the thermal conductivity of bulk MoS_2 (83 W m^{-1}K^{-1}) using first-principles calculations.[17]

Finally, we note that the error bounds on the thermal conductivity obtained here, on the order of ±15%, are larger than typically obtained from TG. We attribute this uncertainty to several factors. First, the laser employed for this work exhibited substantial intensity noise that affected the signal to noise ratio despite the use of balanced detection. Second, wrinkles in the sample may have scattered light and prevented it from reaching the detector. Third, the finite length of delay stage means that data can only be collected to time delays of 13 ns, leading to reduced sensitivity to heat diffusion in the observed signal, particularly for longer grating periods. These effects can be mitigated in the future by improving sample preparation procedures or using chemical vapor deposition for sample fabrication, using a more stable laser source, and performing the real-time TG experiment that employs a continuous-wave probe and a fast oscilloscope rather than a lock-in amplifier. These improvements will be the subject of future work and will lead to substantially reduced uncertainty.

In summary, we have reported measurements of in-plane thermal and elastic properties of free-standing bulk MoS_2 membranes. We obtained a sound velocity of 7000 ± 40 m s^{-1}, which is consistent with recent *ab initio* calculations, and an in-plane thermal conductivity of 74 ± 21 W m^{-1}K^{-1}. Our work provides insights into the in-plane acoustic and thermal properties of MoS_2 and demonstrates the capability of transient grating spectroscopy to characterize other two-dimensional materials that are challenging to study with conventional techniques.

This work was supported by the "GIST-Caltech Research Collaboration" Project through a grant provided by Gwangju Institute of Science and Technology in 2017. T.K. acknowledges the support by the Jeongsong Cultural Foundation (South Korea). D.D. gratefully acknowledges the support by the Agency for Science, Technology and Research (Singapore). The authors thank Stefan Omelchenko,

Dr. Ke Sun, Dr. Hang Zhang, and Dr. Dennis Friedrich for experimental assistance, and Dr. Bo Sun and Andrew B. Robbins for the constructive discussions. The authors also gratefully acknowledge the use of equipment from the Caltech Joint Center for Artificial Photosynthesis (JCAP).

[1] J. A. Wilson and A. D. Yoffe, Adv. Phys. **18**, 193 (1969).
[2] L. F. Mattheiss, Phys. Rev. B **8**, 3719 (1973).
[3] Q. H. Wang, K. Kalantar-Zadeh, A. Kis, J. N. Coleman, and M. S. Strano, Nat. Nanotechnol. **7**, 699 (2012).
[4] A. Kuc, N. Zibouche, and T. Heine, Phys. Rev. B **83**, 245213 (2011).
[5] D. Jariwala, V. K. Sangwan, L. J. Lauhon, T. J. Marks, and M. C. Hersam, ACS Nano **8**, 1102 (2014).
[6] M. Bernardi, M. Palummo, and J. C. Grossman, Nano Lett. **13**, 3664 (2013).
[7] T. S. Sreeprasad, P. Nguyen, N. Kim, and V. Berry, Nano Lett. **13**, 4434 (2013).
[8] M. Kayyalha, J. Maassen, M. Lundstrom, L. Shi, and Y. P. Chen, J. Appl. Phys. **120**, 134305 (2016).
[9] B. Radisavljevic, A. Radenovic, J. Brivio, V. Giacometti, and A. Kis, Nat. Nanotechnol. **6**, 147 (2011).
[10] Z. Jin, Q. Liao, H. Fang, Z. Liu, W. Liu, Z. Ding, T. Luo, and N. Yang, Sci. Rep. **5**, 18342 (2015).
[11] Z. Ding, J.-W. Jiang, Q.-X. Pei, and Y.-W. Zhang, Nanotechnology **26**, 065703 (2015).
[12] Y. Cai, J. Lan, G. Zhang, and Y.-W. Zhang, Phys. Rev. B **89**, 035438 (2014).
[13] X. Gu, B. Li, and R. Yang, J. Appl. Phys. **119**, 085106 (2016).
[14] X. Wang and A. Tabarraei, Appl. Phys. Lett. **108**, 191905 (2016).
[15] W. Li, J. Carrete, and N. Mingo, Appl. Phys. Lett. **103**, 253103 (2013).
[16] Y. Hong, J. Zhang, and X. C. Zeng, J. Phys. Chem. C **120**, 26067 (2016).
[17] D. O. Lindroth and P. Erhart, Phys. Rev. B **94**, 115205 (2016).
[18] X. Wu, N. Yang, and T. Luo, Appl. Phys. Lett. **107**, 191907 (2015).
[19] X. Zhang, D. Sun, Y. Li, G.-H. Lee, X. Cui, D. Chenet, Y. You, T. F. Heinz, and J. C. Hone, ACS Appl. Mater. Interfaces **7**, 25923 (2015).
[20] R. Yan, J. R. Simpson, S. Bertolazzi, J. Brivio, M. Watson, X. Wu, A. Kis, T. Luo, A. R. Hight Walker, and H. G. Xing, ACS Nano **8**, 986 (2014).
[21] A. Taube, J. Judek, A. Łapińska, and M. Zdrojek, ACS Appl. Mater. Interfaces **7**, 5061 (2015).
[22] S. Sahoo, A. P. S. Gaur, M. Ahmadi, M. J.-F. Guinel, and R. S. Katiyar, J. Phys. Chem. C **117**, 9042 (2013).
[23] I. Jo, M. T. Pettes, E. Ou, W. Wu, and L. Shi, Appl. Phys. Lett. **104**, 201902 (2014).
[24] J. Liu, G.-M. Choi, and D. G. Cahill, J. Appl. Phys. **116**, 233107 (2014).
[25] J. L. Feldman, J. Phys. Chem. Solids **37**, 1141 (1976).
[26] K. Kaasbjerg, K. S. Thygesen, and K. W. Jacobsen, Phys. Rev. B **85**, 115317 (2012).
[27] Y. Ding and B. Xiao, RSC Adv. **5**, 18391 (2015).
[28] W. Zhang, Z. Huang, W. Zhang, and Y. Li, Nano Res. **7**, 1731 (2014).
[29] H. Peelaers and C. G. Van de Walle, J. Phys. Chem. C **118**, 12073 (2014).
[30] S. Ge, X. Liu, X. Qiao, Q. Wang, Z. Xu, J. Qiu, P.-H. Tan, J. Zhao, and D. Sun, Sci. Rep. **4**, 5722 (2014).
[31] B. L. Evans and P. A. Young, Proc. R. Soc. London, Ser. A **284**, 402 (1965).
[32] T. Cheiwchanchamnangij and W. R. L. Lambrecht, Phys. Rev. B **85**, 205302 (2012).
[33] E. Fortin and W. M. Sears, J. Phys. Chem. Solids **43**, 881 (1982).
[34] M.-R. Gao, J.-X. Liang, Y.-R. Zheng, Y.-F. Xu, J. Jiang, Q. Gao, J. Li, and S.-H. Yu, Nat. Commun. **6**, 5982 (2015).
[35] Y.-H. Lee, X.-Q. Zhang, W. Zhang, M.-T. Chang, C.-T. Lin, K.-D. Chang, Y.-C. Yu, J. T.-W. Wang, C.-S. Chang, L.-J. Li, and T.-W. Lin, Adv. Mater. **24**, 2320 (2012).
[36] J. A. Rogers, A. A. Maznev, M. J. Banet, and K. A. Nelson, Annu. Rev. Mater. Sci. **30**, 117 (2000).
[37] J. A. Johnson, A. A. Maznev, J. Cuffe, J. K. Eliason, A. J. Minnich, T. Kehoe, C. M. S. Torres, G. Chen, and K. A. Nelson, Phys. Rev. Lett. **110**, 025901 (2013).
[38] J. A. Johnson, A. A. Maznev, M. T. Bulsara, E. A. Fitzgerald, T. C. Harman, S. Calawa, C. J. Vineis, G. Turner, and K. A. Nelson, J. Appl. Phys. **111**, 023503 (2012).
[39] K. Kang, Y. K. Koh, C. Chiritescu, X. Zheng, and D. G. Cahill, Rev. Sci. Instrum. **79**, 114901 (2008).
[40] A. Harata, H. Nishimura, and T. Sawada, Appl. Phys. Lett. **57**, 132 (1990).
[41] J.-Y. Kim, S.-M. Choi, W.-S. Seo, and W.-S. Cho, Bull. Korean Chem. Soc. **31**, 3225 (2010).